

Assessment and Computational Improvement of Thermal Lattice Boltzmann Models Based Benchmark Computations

R. Djebali¹ and M. El Ganaoui²

Abstract: The Lattice Boltzmann method (LBM) became, today, a powerful tool for simulating fluid flows. Its improvements for different applications and configurations offers more flexibility and results in several schemes such as in presence of external/internal forcing term. However, we look for the suitable model that gives correct informations, matches the hydrodynamic equations and preserves some features like coding easily, preserving computational cost, stability and accuracy. In the present work, high order incompressible models and equilibrium distribution functions for the advection-diffusion equations are analyzed. Boundary conditions, acceleration, stability and preconditioning with initial fields are underlined which permit to rigorously selecting two LBGK thermal models. The two selected models are modified, leading to two new schemes going well with the above mentioned computational advantages. The standard and modified schemes have been validated on benchmark computations based two-dimensional natural convection problems for steady flows. First, the standard and modified schemes are intensively tested on a heated differentially air-filled cavity for a wide range of Rayleigh number. Following, we present the predictability level of a selected model based transitional two test cases concerning process of solidification, since these flows types present transition thresholds in the dynamic behaviour. The produced results are compared to high-order accurate solutions in available literature finding results. It is found that the commonly used LB thermal models give similar and consistent results. However, they are time consuming in its standard forms. The modified models show an improvement of the computational cost and permit to suggest an appropriate model based on the most required features in Computational Fluid Dynamics.

Keywords: Lattice Boltzmann method, thermal models, preconditioning, natural convection test cases.

¹ Univ. of Tunis el Manar, FST/LETTM, Tunis 2092, Tunisia. jbelii_r@hotmail.fr

² Univ. of Limoges, SPCTS/CEC, 87068 Limoges, France.

1 Introduction

The computational aspect and its implications for algorithm development in computational fluid dynamics is an important subject since the advancement of powerful and efficient computers [Leung, Berzins (2003); Shu, Ding, Yeo (2005); Tsukiji, Yamamoto (2005)]. These aspects concern numerical integration, polynomial interpolation, mesh generation, moving mesh, algorithm parallelization, hybrid computational approach and especially solvers acceleration. The literature on all these interesting topics is vast [Forth and Staroselsky (2005); El Ganaoui, Bontoux, Lamazouade, Leonardi and de Vahl Davis (2002)]. Besides, the study of natural convection is of particular importance and a broad range of responses was made for numerous applications of classical and recent interest [El Ganaoui, Bontoux, Lamazouade, Leonardi and de Vahl Davis (2002); Liang, Li, Fu and Ma (2009); El Ganaoui and Semma (2009)].

Additionally, numerical simulation and modelling using LB method becomes a challenging branch in CFD [Guo and Zhao (2005); Chatterjee (2010)]. For instance, the LBM enjoys high order accuracy (second order in time and space), efficient computational resources and has met with significant success for numerical simulation and modelling of many classical, complex and flows of current interest [Djebali, El Ganaoui, Sammouda and Bennacer (2009); Djebali, Pateyron, El Ganaoui and Sammouda (2009)]. Recently, the LB method has known an exponential development and appearance of new models and schemes always looking for more improvements. The advances are, usually, made at the additional external/internal terms, the treatment of boundary conditions, the stability, the accuracy and the speeding-up. Such axes are the subject of the present work based on natural convection and heat transfer test cases. The key points and main contents of this paper consist of five sections described as follows: the selection of the equilibrium distribution function for the advection equation, the selection of the equilibrium distribution function for the diffusion equation, the selection of high-order boundary condition treatment, a discuss of the acceleration and the stability of the LB models and finally a results section, where some significant results are achieved.

2 Choice of the equilibrium function for the advection equation

The discrete lattice Boltzmann equation in the presence of body force can be expressed as:

$$f_k(\mathbf{x}', t') - f_k(\mathbf{x}, t) = -\frac{1}{\tau_v} (f_k(\mathbf{x}, t) - f_k^{eq}(\mathbf{x}, t)) + \Delta t S_k \quad (1)$$

The choice of the appropriate form for the forcing term S_k has been studied by [Mohamad, Kuzmin (2010)]. The authors concluded that the source/sink term $S_k =$

$w_k \mathbf{e}_k \cdot \mathbf{F} / c_s^2$ (where \mathbf{F} is the body force) shows more better results compared to other schemes. Such a form will be adopted in the present study.

The macroscopic density and velocity are computed in a 9-bits lattice as:

$$\begin{bmatrix} \rho(\mathbf{x}, t) \\ \rho \mathbf{u}(\mathbf{x}, t) \end{bmatrix} = \sum_{k=0,8} \begin{bmatrix} f_k \\ \mathbf{e}_k f_k \end{bmatrix} \quad (2)$$

In the literature, the equilibrium density distribution function $f_k^{eq}(\mathbf{x}, t)$ has undergone some modifications looking for eliminating the compressibility effects due to the LB method itself. In LB modelling and simulation, the following three models are usually adopted:

- The completely incompressible model due to [Guo, Shi and Zheng, (2002)], written as:

$$f_k^{eq}(\mathbf{x}, t) = \begin{cases} -4\sigma p + s_0(u), & k = 0 \\ \lambda p + s_k(u), & k = 1, 4, \\ \eta p + s_k(u), & k = 5, 8 \end{cases} \quad (3)$$

$$s_k(u) = \omega_k [3 \mathbf{e}_k \cdot \mathbf{u} + 4.5 (\mathbf{e}_k \cdot \mathbf{u})^2 - 1.5 u^2],$$

$$\sigma = 5/12, \lambda = 1/3 \text{ and } \eta = 1/12$$

The macroscopic pressure and velocity are, computed as:

$$\begin{cases} p(\mathbf{x}, t) = \frac{3}{5} \left(\sum_{k=1,8} f_k - \frac{2}{3} \mathbf{u}^2 \right) \\ \mathbf{u}(\mathbf{x}, t) = \sum_{k=1,8} \mathbf{e}_k f_k \end{cases} \quad (4)$$

- The incompressible model due to [He, Luo, (1997)], written as:

$$f_k^{eq}(\mathbf{x}, t) = \omega_k \rho + \rho_0 s_k(\mathbf{u}) \quad (5)$$

and the macroscopic variables are computed as:

$$\begin{bmatrix} \rho(\mathbf{x}, t) \\ \rho_0 \mathbf{u}(\mathbf{x}, t) \end{bmatrix} = \sum_{k=0,8} \begin{bmatrix} f_k \\ \mathbf{e}_k f_k \end{bmatrix} \quad (6)$$

- The commonly used compressible model (in the limit of $\text{Ma} \rightarrow 0$, where Ma is the Mach number) written as:

$$f_k^{eq}(\mathbf{x}, t) = \rho (\omega_k + s_k(\mathbf{u})) \quad (7)$$

where the macroscopic density and velocity are computed as in equation (2).

For all the cited schemes, the relaxation times τ_v is linked to the kinetic viscosity as $\tau_v = 3\nu + 0.5$.

It is worth-noting that in the He's model, the compressible effect is reduced effectively by explicitly eliminating the terms of order $o(Ma^2)$, and both the Guo's model (first) and the He's model (second) are theoretically the most appropriate for steady and unsteady dynamic flows. In several tests (not presented here), we have found that the He's model shows some difficulties in thermal flows simulated using LB double population models for high Reynolds and Rayleigh numbers. The third model has been used in many complex applications (for steady and unsteady flow) and has found to give reliable results compared to classical discretization methods [Peng, Shu and Chew (2003); Chew, Shu and Niu (2002)]. It has been, also, extensively verified, used and has shown better performance in 2D and 3D simulations [Shu, Niu and Chew (2003)]. For these reasons and for its simple scheme (compared to the incompressible Guo's model) it will be adopted in the following, under same rigor modifications.

3 Choice of the equilibrium distribution for the diffusion equation

For the double population thermal approach, three models are commonly used. That depends mainly on the used lattice (m-bits) or the equilibrium distribution. The governing equation for the diffusion equation is written as:

$$h_k(\mathbf{x}', t') - h_k(\mathbf{x}, t) = -\frac{1}{\tau_\alpha} (h_k(\mathbf{x}, t) - h_k^{eq}(\mathbf{x}, t)) \quad (8)$$

- The simple way is to use a 9-bits lattices (m=9) as for the dynamic field and for a simple coding: since we will use the same streaming subroutines, the same weighting factors w_k and the same velocity vectors \mathbf{e}_k for the two distributions. The temperature equilibrium distribution function for the titled passive scalar approach will be:

$$h_k^{eq}(\mathbf{x}, t) = T(\mathbf{x}, t)(\omega_k + s_k(\mathbf{u})) \quad (9)$$

the macroscopic temperature is computed as:

$$T(\mathbf{x}, t) = \sum_{k=0,8} h_k \quad (10)$$

The corresponding relaxation time τ_α is linked to the thermal diffusivity as $\tau_\alpha = 3\alpha + 0.5$.

- The simplified thermal energy model (STEM) proposed by [Peng, Shu and Chew (2003)], for the energy equation, has been also extensively used and has shown great features. Its equilibrium distribution function is written as:

$$h_k^{eq} = \omega_k \rho \varepsilon \left(1.5(\mathbf{e}_k^2 - u^2) + 3(1.5\mathbf{e}_k^2 - 1)(\mathbf{e}_k \cdot \mathbf{u}) + 4.5(\mathbf{e}_k \cdot \mathbf{u})^2 \right) \quad (11)$$

where $\varepsilon = DRT/2$, $D = 2$ and $R = 1$. The macroscopic temperature is computed as:

$$\rho \frac{DR}{2} T(\mathbf{x}, t) = \sum_{k=0,8} h_k \quad (12)$$

The corresponding relaxation time τ_α is linked to the thermal diffusivity as $\tau_\alpha = 1.5\alpha + 0.5$. A 4-bits STEM was proposed by [Azwadi, Sidik (2007)], but it will not be considered here for lack of accuracy.

- The 4-bits passive scalar model is more recommender by [Mohamad (2007)] based on the idea that the diffusion equation are linear on velocity. This model has been, also, used by [Djebali, Pateyron, El Ganaoui and Sammouda (2009)] for very high temperature jet flows and has shown great efficiency. The corresponding equilibrium distribution function is expressed as follows:

$$h_k^{eq}(\mathbf{x}, t) = 0.25 T(\mathbf{x}, t) [1 + 2 \mathbf{e}_k \cdot \mathbf{u}] \quad (13)$$

the macroscopic temperature is computed as:

$$T(\mathbf{x}, t) = \sum_{k=1,4} h_k \quad (14)$$

The corresponding relaxation time τ_α is linked to the thermal diffusivity as $\tau_\alpha = 2\alpha + 0.5$.

We have to mention here, that the first thermal 9-bits approach is memory consuming since the LBM needs to memorize nine values per variable (over against 4 for the D2Q4 model); and is time consuming since the collision process takes about 70% per time step (it takes five additional operations over against the D2Q4 model). Furthermore, it has been demonstrated in [Peng, Shu and Chew (2003)] that the second 9-bits form (STEM) is more efficient in the computational cost. For these raisons, the first 9-bits thermal model will be discarded and we will consider in the following the D2Q4 passive scalar model and the 9-bits STEM model. A rigorous comparison will be carried out between the D2Q9-STEM form and the D2Q4 one to determine each features based on the test problems. The two models will be:

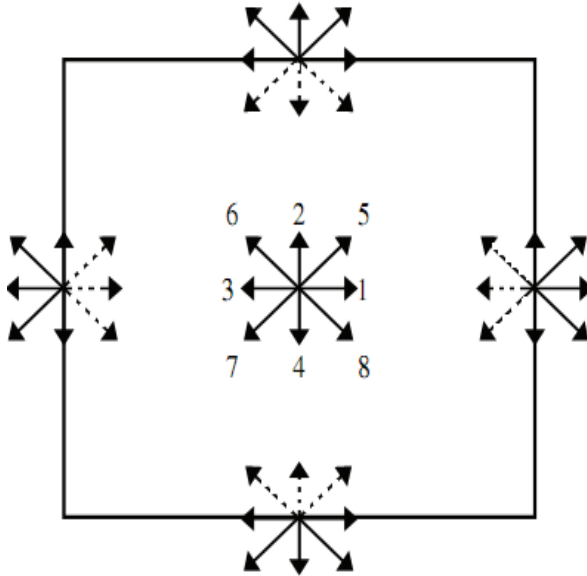


Figure 1: Boundary condition treatment for D2Q9 lattice. Continuous: known and dashed: unknown functions at wall node.

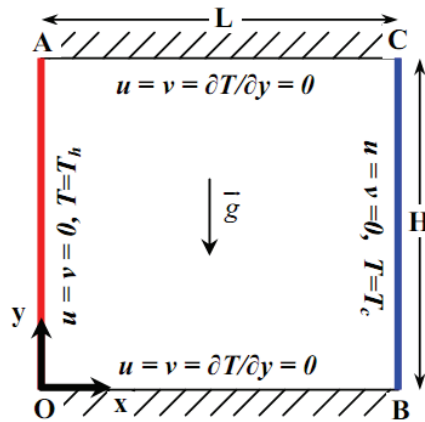


Figure 2: Geometry and boundary conditions of natural convection problem in a square cavity.

-Model 1: a double population based on different lattices, D2Q9-D2Q4 for the dynamic and thermal fields respectively:

$$\begin{cases} f_k^{eq}(\mathbf{x}, t) = \rho(\omega_k + s_k(\mathbf{u})), & k = 0, 8 \\ h_k^{eq}(\mathbf{x}, t) = 0.25T[1 + 2\mathbf{e}_k \cdot \mathbf{u}], & k = 1, 4 \end{cases} \quad (15)$$

and the macroscopic variables are computed using the equations (2) and (14).

- Model 2: a double population based on the same 9-bits lattice for the dynamic and thermal fields, D2Q9-D2Q9:

$$\begin{cases} f_k^{eq}(\mathbf{x}, t) = \rho(\omega_k + s_k(\mathbf{u})) \\ h_k^{eq} = \omega_k \rho \varepsilon (1.5(\mathbf{e}_k^2 - u^2) + 3(1.5\mathbf{e}_k^2 - 1)(\mathbf{e}_k \cdot \mathbf{u}) + 4.5(\mathbf{e}_k \cdot \mathbf{u})^2) \end{cases}, k = 0, 8 \quad (16)$$

and the macroscopic variables are computed using the equations (2) and (12).

4 Boundary condition treatment

Implementation of boundary condition is an important issue in the LB method. In general case, there are two classes of boundary conditions: the free boundary condition (periodic boundary, open boundary and moving boundary) and the solid boundary condition (non-slip boundary, slip boundary). The treatments differ from one problem to other. We discuss in here the quite simple and commonly used schemes. For the present problem, the non-slip boundary condition is adopted at the four walls and the bounce-back rule will be adopted.

As one can see for the left wall (Fig. 1), the distributions functions f_6 , f_3 and f_7 (solid) are determined by the streaming process. However the incoming ones (dashed), f_1 , f_5 and f_8 are unknown and are determined using standard bounce-back rule as: $f_1 = f_3$, $f_5 = f_7$ and $f_8 = f_6$.

The same treatment is applied to the unknown distributions functions (dashed vectors) at all nodes of the other walls. In spite of its simplicity, some authors claim that this scheme is first order accurate which can alter the accuracy of second order in LBM.

A second order accurate scheme is the bounce-back of the non-equilibrium part, expressed as $f_\alpha^{neq} = f_\beta^{neq}$. For the unknown functions, we have:

$$\begin{cases} f_1 = f_3 + (f_1^{eq} - f_3^{eq}) \\ f_5 = f_7 + (f_5^{eq} - f_7^{eq}) \\ f_8 = f_6 + (f_8^{eq} - f_6^{eq}) \end{cases} \quad (17)$$

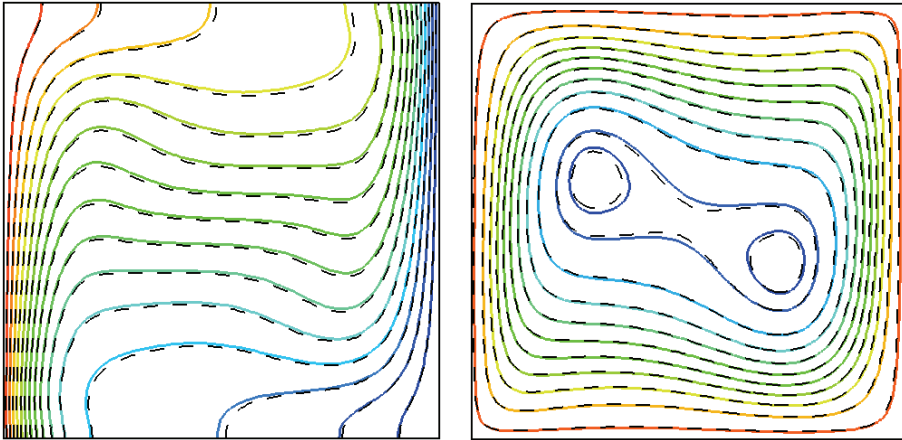


Figure 3: Contour-maps of isotherms (left) and streamlines (right) for the model I (dashed) and model II (solid) for $Ra=10^5$.

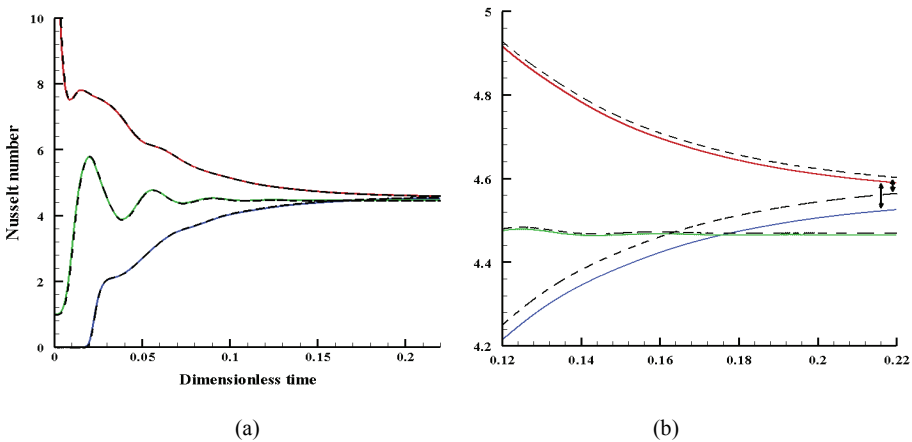


Figure 4: (a) Time history of the Nusselt numbers at the hot wall (red), at the cold wall (blue) and throughout the cavity (green). Dashed line: model I, continuous line: model II; (b) zoomed part near the established regime, $Ra=10^5$.

The bounce-back rule of the non-equilibrium part is also adopted for the STEM thermal model, and is expressed as:

$$h_{\alpha}^{neq} - \bar{e}_{\alpha}^2 f_{\alpha}^{neq} = -(h_{\beta}^{neq} - \bar{e}_{\beta}^2 f_{\beta}^{neq}) \tag{18}$$

where α and β are two opposite directions at a wall node, α incoming and β outgoing. The bounce-back rule of the non-equilibrium part for the passive scalar thermal model is expressed as:

$$h_{\alpha}^{neq} = h_{\beta}^{neq} \quad (19)$$

The wall temperatures are used for the calculation of the equilibrium parts and the Neumann boundary condition is solved by the classical second order finite differencing. The bounce-back rule of the non-equilibrium parts will be used in the following.

5 Acceleration and stability

The lattice Boltzmann equation is valid for the limit $\tau > 0.5$. For the two limits $(0.5, \infty)$, we have code divergence or non physical oscillations. To overcome the unphysical oscillations, [Hui and ChuiJie (2009)] introduce a modification in the relaxation time expression as: $\tau_v = 3\nu/\theta + 1 - 0.5/\theta$, where θ is a weighting coefficient. The post-collision distribution function is computed as:

$$\bar{f}(\mathbf{x}, t + \Delta t) = \theta f(\mathbf{x}, t + \Delta t) + (1 - \theta)f(\mathbf{x}, t) \quad (20)$$

One must choose θ under the condition $\tau_v > 0.5$ which introduces new constraint. An intuitive model, originally proposed by [Guo, Zhao and Shi (2004)] and extended by [Premnath, Pattison and Banerjee (2009)] to flow with body force, offers more stability to the LB method, allows accurate results for coarser grid-size and speeds-up the convergence for steady flows or the established regime for unsteady flows. The model is quite simple compared to other techniques of acceleration (such as Multi-Grid Technique). At our best knowledge, this study is the first extension of this technique to thermal flows.

The models 1 and 2 will be modified respectively to models I and II including accelerating coefficients as:

- Model I:

$$\begin{cases} f_k^{eq}(\mathbf{x}, t) = \omega_k \rho (1 + 3 \mathbf{e}_k \cdot \mathbf{u} \\ \quad + (4.5(\mathbf{e}_k \cdot \mathbf{u})^2 - 1.5u^2)/\gamma_f), \quad k = 0, 8 \\ h_k^{eq}(\mathbf{x}, t) = 0.25 T (1 + 2 \mathbf{e}_k \cdot \mathbf{u}/\gamma_h), \quad k = 1, 4 \end{cases} \quad (21)$$

and the corresponding relaxation times become $\tau_v = 3\nu/\gamma_f + 0.5$ and $\tau_{\alpha} = 2\alpha/\gamma_h + 0.5$.

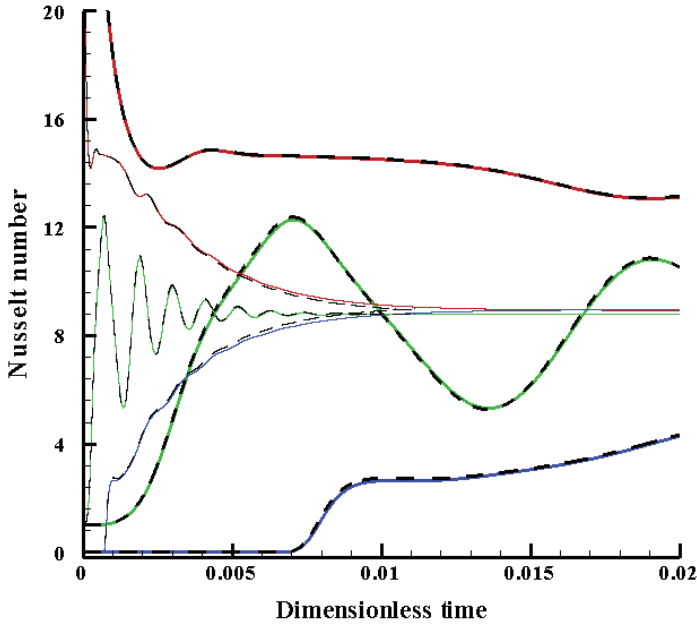


Figure 5: Time history of the Nusselt numbers for $Ra=10^6$ at the hot wall (red), at the cold wall (blue) and throughout the cavity (green). Dashed line: model I, continuous line: model II, bold: $\gamma=1$, fin: $\gamma=0.1$.

-Model II:

$$\begin{cases} f_k^{eq} = \omega_k \rho (1 + 3 \mathbf{e}_k \cdot \mathbf{u} + (4.5(\mathbf{e}_k \cdot \mathbf{u})^2 - 1.5u^2)/\gamma_f) \\ h_k^{eq} = \omega_k \rho \epsilon 3 (1.5(\mathbf{e}_k^2 - u^2/\gamma_h) + [(1.5\mathbf{e}_k^2 - 1)(\mathbf{e}_k \cdot \mathbf{u}) + 4.5(\mathbf{e}_k \cdot \mathbf{u})^2]/\gamma_h) \end{cases}, k = 0, 8 \quad (22)$$

and the corresponding relaxation times become $\tau_v = 3v/\gamma_f + 0.5$ and $\tau_\alpha = 1.5\alpha/\gamma_h + 0.5$.

Following the modified equilibrium thermal distribution, the preconditioned internal energy equation is derived using the Chapman-Enskog procedure (see Appendix A). It is noted that the Mach number becomes $Ma^* = Ma/\gamma_f^{0.5}$ and the accuracy of the models I and II is linear function of v/γ_f and α/γ_h compared to the standard models 1 and 2 [Premnath, Pattison and Banerjee (2009)].

6 Results

In this section three test cases are investigated. All cases interested flow and heat transfer problems for different topics and are based on different two-dimensional configurations. The reference scales used for length, velocity and time are (respectively) H , α/H and H^2/α . All the calculations are performed on the computing server CALI (CALcul en LIMousin). To conduct rigorous comparison in any simulation test, the routines of the two models I and II are launched simultaneously (in parallel).

Test case 1: Side wall heated cavity (steady)

The natural convection problem in a square cavity is presented in Fig. 2. The cavity is of $L \times H$ dimensions ($L=H$). To describe the convective heat transfer we use the averaged Nusselt numbers at the hot wall \overline{Nu}_h , at the cold wall \overline{Nu}_c and in the whole domain \overline{Nu} , expressed as:

$$\overline{Nu}_h = \frac{1}{\alpha \Delta T / H} \frac{1}{H} \int_0^H (uT - \alpha (\partial T / \partial x))|_{x=0} dy \tag{23}$$

$$\overline{Nu}_c = - \frac{1}{\alpha \Delta T / H} \frac{1}{H} \int_0^H (uT - \alpha (\partial T / \partial x))|_{x=L} dy \tag{24}$$

$$\overline{Nu} = \frac{1}{L} \int_0^L \overline{Nu}_h dx \tag{25}$$

The convergence criteria used for the steady state is expressed as:

$$\left| \frac{\overline{Nu}(t + 5000) - \overline{Nu}(t)}{\overline{Nu}(t)} \right| \leq 10^{-4} \tag{26}$$

Tab. 1 summarizes the present results for $Ra=10^5$ for the Models I and II taking $\nu=0.01$ and $\gamma_f = \gamma_h = \gamma = 1$ and different grid sizes. For convenience, the number of iterations is expressed in unit of 5000 due to the convergence criteria checked after each 5000 iterations. High order accurate reference results using FV method and GDQ method are gathered for seek of comparison. The tested fields are the maximal horizontal velocity at mid-width and its location, the maximal vertical velocity at mid-height and its location, the maximal stream-function value and the averaged Nusselt number throughout the cavity. Our results are expressed with four digits float.

In the quantitative sense, one can see that the two models give very close results for all the tested fields. Increasing the grid size the results are well improved compared to references results. For the model II, better results can be obtained with finer grids

as given in [Peng, Shu and Chew (2003)]. Qualitatively (see Fig. 3), the isotherms and iso-stream-functions distributions show that the two models give the same or very similar results.

For the computational cost, the model II generally takes few additionally iterations to achieve steady state. That can be easily remarked from Fig. 4 (a), the time histories of the Nusselt numbers \overline{Nu}_h , \overline{Nu}_c and \overline{Nu} are undistinguishable. The zoomed part near the established regime (Fig. 4 (b)) shows that \overline{Nu}_h and \overline{Nu}_c , for the model I, converge to the same value 4.5842 faster than the model II, which agrees well with the iterations numbers taken for a grid size of 150x150. However, although both models converge to almost the same number of iterations, the CPU times differ considerably: Model I preserves much the computational time (see Tab. 1).

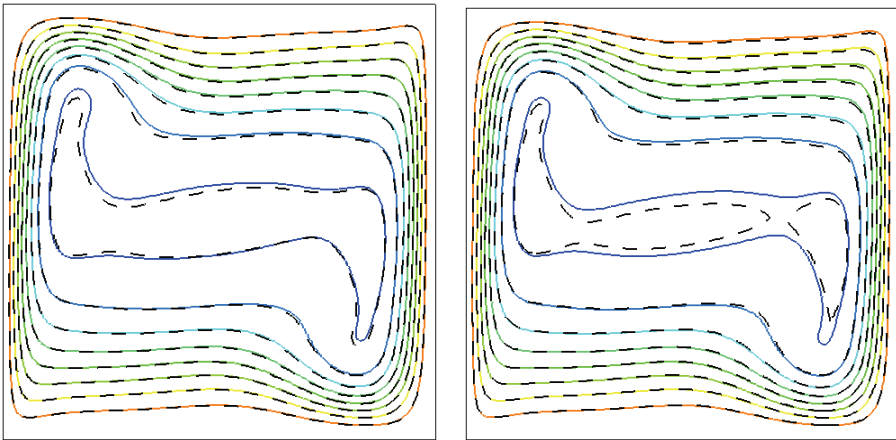


Figure 6: Contour-maps of isotherms for $Ra=10^6$. left: model I, right: model II, solid: $\gamma=1$, dashed: $\gamma=0.1$.

In the second part of this section we discuss the effect of the preconditioning parameters γ . The Rayleigh number is chosen to be 10^6 , the lattice kinetic viscosity and thermal diffusivity are chosen to equal 0.0075 and for the preconditioning parameter, we examine the cases $\gamma_f = \gamma_g = 1$ and 0.1. It is noted above that when $\gamma < 1$ the accuracy will be affected by the ratio ν/γ . Then, one must choose a new kinetic viscosity and thermal diffusivity. We found that it is more intuitive to keep invariant the Mach number (0.102); then, for the present test the new viscosity and thermal diffusivity change from 0.0075 at $\gamma=1$ to 0.00237 at $\gamma=0.1$. The results are presented in Tab. 2.

For $\gamma=1$, it is well seen that (i) the two models show a high level of predictability,

Table 1: Comparison of the present LBM predictions with the numerical solutions of references Ref.1 and Ref.2 for $Ra=10^5$, 'x' denotes: x5000 iterations. Ref.1: [de Vahl Davis (1983)] and Ref.2: [Shu, Xue (1998)].

| Lattice | Model | U_{max} | y | V_{max} | x | ψ_{max} | \bar{Nu} | iter. | CPU(s) |
|---------|-------|-----------|--------|-----------|--------|--------------|------------|-------|---------|
| 100^2 | I | 34.5588 | 0.8500 | 68.0857 | 0.0700 | 9.5543 | 4.4706 | 49 x | 672.96 |
| | II | 34.6873 | 0.8500 | 68.1364 | 0.0700 | 9.5751 | 4.4618 | 47 x | 831.12 |
| 150^2 | I | 34.6963 | 0.8533 | 68.4569 | 0.0667 | 9.5877 | 4.4915 | 91 x | 2842.40 |
| | II | 34.7475 | 0.8533 | 68.5756 | 0.0667 | 9.6042 | 4.4887 | 94 x | 3868.26 |
| | Ref.1 | 34.722 | 0.855 | 68.590 | 0.066 | 9.612 | 4.519 | - | - |
| | Ref.2 | 34.736 | 0.855 | 68.640 | 0.065 | 9.618 | 4.523 | - | - |

Table 2: Comparison of the present results for $Ra=10^6$ predicted using standard models ($\gamma=1$) and accelerated models ($\gamma=0.1$), 'x' denotes: x5000 iterations. The two findings are also compared to references Ref.1: [de Vahl Davis (1983)] and Ref.2: [Shu, Xue (1998)].

| Lattice | Model | γ | U_{max} | y | V_{max} | x | \bar{Nu} | iter. | CPU(s) |
|---------|-------------------|----------|-----------|--------|-----------|--------|------------|-------|---------|
| 150^2 | I | 1 | 64.3298 | 0.8533 | 218.4357 | 0.0399 | 8.7328 | 79 x | 2459.22 |
| | II | 1 | 64.5907 | 0.8533 | 218.4111 | 0.0399 | 8.6920 | 77 x | 3159.00 |
| 200^2 | I | 1 | 64.6416 | 0.8500 | 219.3287 | 0.0399 | 8.7633 | 120 x | 6961.89 |
| | II | 1 | 64.7223 | 0.8500 | 219.2961 | 0.0399 | 8.7390 | 123 x | 9430.67 |
| 150^2 | I | 0.1 | 63.5481 | 0.8533 | 216.2578 | 0.0399 | 8.8043 | 30 x | 941.25 |
| | II | 0.1 | 64.4013 | 0.8600 | 216.6580 | 0.0399 | 8.7194 | 30 x | 1317.20 |
| 250^2 | I | 0.1 | 64.3910 | 0.8480 | 218.7332 | 0.0399 | 8.8041 | 67 x | 6417.93 |
| | II | 0.1 | 64.8949 | 0.852 | 218.8855 | 0.0399 | 8.7702 | 69 x | 9168.07 |
| | Ref. ¹ | - | 64.630 | 0.850 | 219.360 | 0.0379 | 8.800 | - | - |
| | Ref. ² | - | 64.775 | 0.850 | 220.640 | 0.0350 | 8.800 | - | - |

(ii) as for $Ra=10^5$, the two standard models ($\gamma=1$) takes roughly the same number of iterations to achieve the established regime, but the model I is clearly very fast (it has less CPU time), (iii) increasing the grid size from 150^2 to 200^2 , the accuracy of the results is enhanced for the two models compared to the referenced results and the CPU times are increased significantly.

For $\gamma = 0.1$, let us first choose a grid size of 150^2 for the two test models. The predictions are found to be in good agreement with references results. Furthermore, the CPU time is significantly decreased as shown in Tab. 2 and through the time histories in Fig. 5. The comparison between the standard forms ($\gamma=1$) and the modified ones ($\gamma=0.1$) is shown in Fig. 6. Near the walls, the two models represent similarly the streamlines and isotherms structures. At the cavity core, the results of the accelerated schemes undergo a slight deformation which affects the calculated fields in Tab.2. The model II, as mentioned for $Ra=10^5$, takes more CPU time to

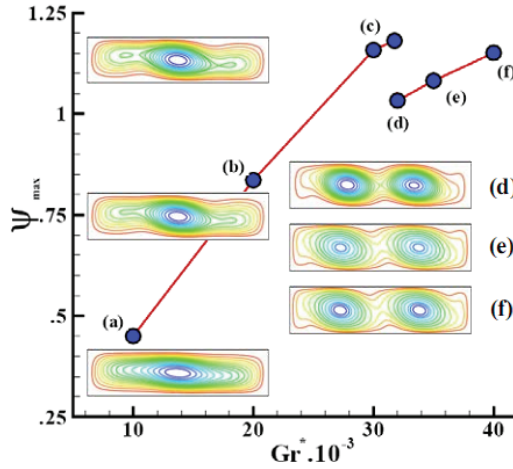


Figure 7: Bifurcation diagram for the horizontal Bridgman model (fixed interface) for $Pr = 0.015$.

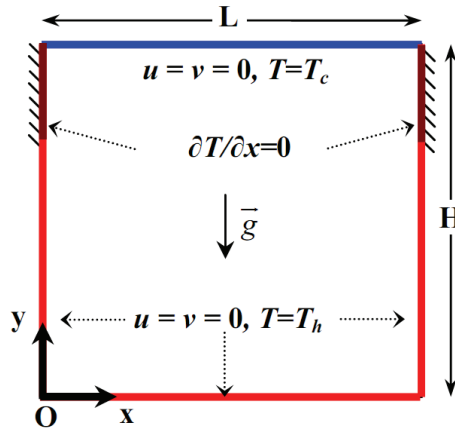


Figure 8: Simplified vertical Bridgman configuration with fixed interface.

achieve the steady state.

The main idea of this part is to demonstrate that in general cases, for high flow parameters (Rayleigh, Reynolds, . . .), one must choose low values for the kinetic viscosity, which is not allowed due to the instability limit $\tau > 0.5$. The parameter γ can be, then, optimized to obtain acceptable results with coarse grid sizes or accurate results with fine grid size with speeding-up the established regime and

keeping more stability which are important issues in CFD. This is well shown in Tab. 2: for a grid size of 250^2 , $\gamma=0.1$ and $\nu=0.005$ the predicted results are the best and are close to reference results. However, the CPU time, for the two models, is clearly decreased compared to the standard forms using even a grid size of 150^2 .

To determine the speeding-up law of the preconditioning parameter γ , we assume that its effect results in a power law, ie $\text{CPU}(\gamma)=C \cdot \gamma^a$ where C and a are two parameters. The computations for $\text{Ra}=10^6$ and a grid size 150 (see Tab. 3) are used to calculate the coefficient a for the two models. The estimations lead to $a_I=0.4173$ and $a_{II}=0.3801$. These two values agree well with the value $a \approx 0.45$ found previously by [Guo, Zhao, Shi (2004)].

The third part of this study focuses on the comparison of two ways of accelerating the established regime. The Rayleigh number is chosen to be 10^7 and the grid size is 250^2 . The first way is the above tested procedure using the preconditioning parameter γ (with $\gamma=0.1$ and $\nu=0.00158$), the second way is to use an initial non zero-fields (with $\gamma=1$ and $\nu=0.005$). The adopted initial solution is the steady state solution corresponding to $\text{Ra}=10^6$ using a grid size of 250^2 . Tab. 3 summarizes the predicted results. It is clear that the acceleration technique using non-zero initial fields is as effective and preserves significantly computational time. In fact and first, the CPU time taken for $\text{Ra}=10^7$ with a grid size 250^2 (Tab. 3) is much lower than that taken for $\text{Ra}=10^6$ using a grid size 200^2 (Tab. 2): 4182.75 sec. for $\text{Ra}=10^7$ counter 6961.89 for $\text{Ra}=10^6$. Second, the CPU times for the two models is much lower using the acceleration by means of non-zero initial field than the acceleration using the preconditioning parameter γ as depicted in Tab. 3. However, this technique has the disadvantage that the time saved in the computation at $\text{Ra}=10^7$ has been lost to prepare the initializing solution for $\text{Ra}=10^6$. For this reason, preconditioning the computation using the parameter γ is more efficient to save more computational time for all. The two models results keep the same features discussed above for $\text{Ra}=10^5$ and $\text{Ra}=10^6$.

In the following the two accelerated models will be considered versus discretization approaches to solve problems interesting directional solidification industry. The problems consider two situations with symmetry breaking for low Prandtl number fluids flowing in enclosures: the horizontal and the vertical Bridgman models. Further explanations for the two transitional test cases definitions can be found in [El Ganaoui, Djebali (2010); Djebali, Sammouda, El Ganaoui (2010)].

In the following two case-tests, the focus is put on the predictability level of the modified LB model in the results rather than to describe the models in details.

Test case 2: Transitions thresholds in the horizontal Bridgman model

In this test case, we consider the horizontal Bridgman cavity. The simplified model

is the same as in Fig. 2, with an aspect ratio $A = L/H = 4$. The cavity is filled with Gallium of Prandtl number 0.015, the resolution is taken 320x80 and the preconditioning parameter γ is chosen 0.1 for the two relaxation times. The simplified model considers a fixed interface, maintained at constant temperatures as for former established benchmarks. This flow is characterized by a transition in the dynamic structure behaviour at low Grashof numbers Gr^* , where $Gr^* = Ra/Pr$ (Gr^* is the modified Grashof number, see [Gelfgat, Bar-Yoseph, Yarin (1999)]). The zero initial conditions are taken for all the computed fields. The LB results (model 1) for the maximum stream-function magnitude vs the Grashof number Gr^* are summarized in Tab. 4.

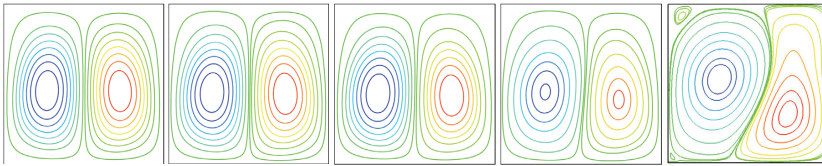


Figure 9: Symmetry breaking for the simplified vertical Bridgman model, $Pr=0.01$.

For $Gr=10^4$, the flow is a one convective clock-wise rotating cell. A transition occurs at a critical value of $Gr \approx 31750$ and the flow structure is a three counter-rotating cells. In the vicinity of the critical point the Grashof number is increased uniformly (by a step of 250). For $Gr=32000$, the flow exhibits a three cells structure. However, for $Gr=32250$ a new transition characterized by two-cell structure is identified. The present results are gathered with previous solutions [Gelfgat, Bar-Yoseph, Yarin (1999); Ben Hadid, Roux (1990); Pulicani, del Arco, Randriamampianina, Bontoux, Peyret (1990)]; Winters (1988); Winters (1990)] in Tab. 5. The bifurcations diagram defined by the plot of maximum stream-function magnitude vs the Grashof number is presented in Fig. 7. The regime remains steady with two rolls until $Gr=35000$. A change in the cells-shape is observed near isothermal walls for $Gr=40000$, the stream-function magnitude increases considerably and no time dependency is remarked. This behaviour defines a new branch with two cells in the flow patterns. One can remark the excellent agreement between the LB results and those of the traditional methods in CFD. It can be concluded, through this test case, that the present modified LB model is a promising alternative for transition thresholds at low Prandtl numbers flows, as it accurately captures the threshold of transition even for coarser grid compared to the standard model used in [28].

Test case 3: Symmetry breaking behaviour in vertical Bridgman model

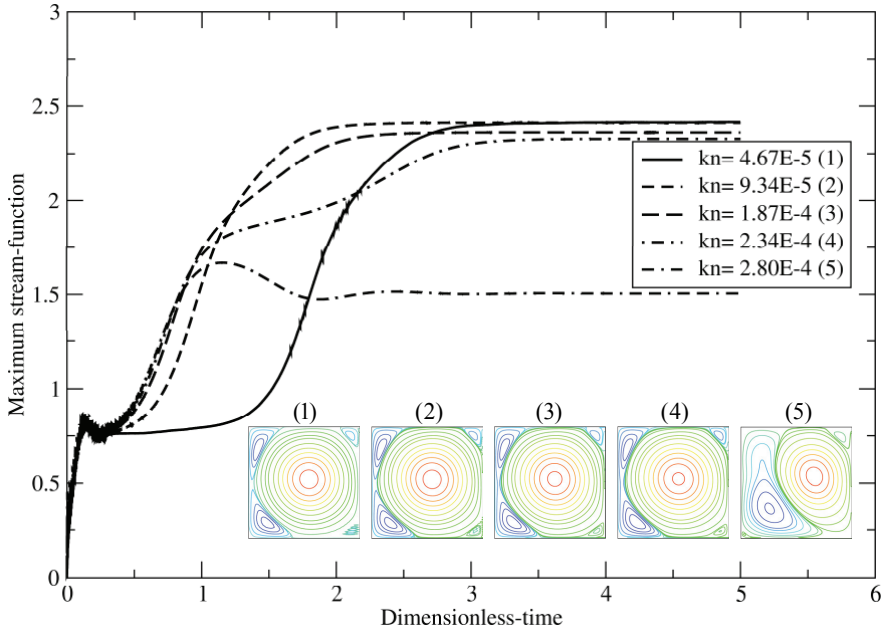


Figure 10: Maximum dimensionless stream-function magnitude vs dimensionless time for $Gr=6 \cdot 10^5$ and different Knudsen numbers.

In this third test case, the modified LB first model is tested based simplified model of the classical vertical Bridgman technique as depicted in Fig. 8. The cavity is filled with a material of a Prandtl number $Pr=0.01$ and the resolution is chosen to be 100×100 . The preconditioning parameter γ is chosen 0.1 for the two relaxation times.

Table 3: Comparison between preconditioned models ($\gamma=0.1$) and results with non-zero initial fields for $Ra=10^7$, ‘x’ denotes: x5000 iterations, ‘*’ denotes. initialized by the $Ra=10^6$ steady’s solution. Ref.: [Le Quéré (1991)]

| Lattice | Model | γ | Ψ_{max} | \bar{Nu}_h | \bar{Nu}_c | \bar{Nu} | iter. | CPU(s) |
|---------|-------|----------|--------------|--------------|--------------|------------|-------|---------|
| 250^2 | I | 1* | 30.7951 | 16.5140 | 16.8165 | 16.3593 | 45 x | 4182.75 |
| | | 0.1 | 29.9133 | 16.3613 | 17.2182 | 16.5568 | 61 x | 5925.38 |
| 250^2 | II | 1* | 30.8918 | 16.4285 | 16.4989 | 16.4157 | 46 x | 5577.18 |
| | | 0.1 | 29.9929 | 16.8432 | 16.8074 | 16.4880 | 59 x | 8353.73 |
| | | [Ref.] | 30.165 | 16.523 | 16.523 | 16.523 | - | - |

Table 4: Estimation of Hopf point, maximum stream-function magnitude vs modified Grashof number.

| | | | | | | | |
|------------------|-------|-------|-------|-------|-------|-------|-------|
| $Gr^*=Gr/A.10^3$ | 10 | 20 | 30 | 32 | 32.25 | 35 | 40 |
| $ \Psi_{max} $ | 0.450 | 0.836 | 1.158 | 1.181 | 1.033 | 1.082 | 1.151 |

Table 5: Hopf point estimated for A=4 and Pr=0.015 with various methods: Ref.1: [Gelfgat, Bar-Yoseph, Yarin (1999)], Ref.2: [Ben Hadid, Roux (1990)], Ref.3: [Pulicani, del Arco, Randriamampianina, Bontoux, Peyret (1990)], Ref.4: [Winters (1988)], Ref.5: [Winters (1990)] and (*): model 1.

| Method | Spectral [Ref.1] | FVM [Ref.1] | FDM [Ref.2] | Spectral [Ref.3] | FEM [Ref.4,5] | LBM Present (*) |
|---------------------|------------------|-------------|-------------|------------------|---------------|-----------------|
| Mesh | 200x100 | 60x24 | 121x41 | 40x30 | 66x24 | 320x80 |
| Gr.10 ⁻³ | 32.996 | 32.5-33.5 | 32.5-33.5 | 33.3 | 33.002 | 32.0 |

Table 6: Symmetry breaking and routes to unsteadiness in vertical Bridgman growth for Pr=0.01: comparison with various Ref.1: [results, Larroudé, Ouazzani, Alexander, Bontoux (1994)], Ref.2: [Bennacer, El Ganaoui, Leonardi (2006)], Ref.3: [Semma (2004)].

| Method | Symmetric, $\Psi_{max}(Gr=2 \cdot 10^5)$ | Gr_c of transition SS-AS |
|-------------------|--|----------------------------|
| Spectral [Ref.1] | - | 2.5-3 10^5 |
| FV (3D) [Ref.2] | - | 3 10^5 |
| FV (2D) [Ref.3] | 0.290 | 3.50 10^5 |
| LBM (2D): Present | 0.267 | 2.85-3 10^5 |

The model exhibits a rapid change in boundary conditions, and the onset of the flow results from the Rayleigh-Bénard configuration. For low values of Grashof number, the flow is a steady symmetric structure (SS) showing two counter-rotating cells. Enhancing the heat transfer by increasing the Grashof number, the maximum stream-function magnitude ψ_{max} is 0.267, 0.275, 0.356, 0.364 and 0.340 (in unit of thermal diffusivity) for respectively $Gr=2 \cdot 10^5$, $2.5 \cdot 10^5$, $2.75 \cdot 10^5$, $2.85 \cdot 10^5$ and $3 \cdot 10^5$, then the stream-function magnitude reaches its maximum for a Grashof number ranged between $2.85 \cdot 10^5$ and $3 \cdot 10^5$. The flow becomes completely asymmetric (SAS) for $Gr=3 \cdot 10^5$ and indicates a change in the flow pattern characterized by a typical symmetry breaking in the melt flow structure (see Fig. 9). The present LB first model results are confirmed by the 2D Spectral results [Larroudé, Ouazzani, Alexander, Bontoux (1994)] where transition threshold is identified between $2.5 \cdot 10^5$ and $3 \cdot 10^5$ and FV ones (2D and 3D) [Bennacer, El Ganaoui, Leonardi (2006)];

Semma (2004)]. A recapitulative table gathers each results with the used method (see Tab. 6).

The convergence dimensionless time is about 10 in unit of the thermal diffusion time scale based the cavity height H^2/α .

With more increase of Grashof number, the flow becomes steady and absolutely asymmetric (SAS). Moreover, we observed the growth progressively of one roll and the reduction of the other. We have remarked that this behaviour depends strongly on the Knudsen number defined as follows:

$$Kn = \sqrt{\pi \sigma / 2} \cdot v^* / (c_s H) \quad (27)$$

Where σ is the heat capacity ratio for a monatomic ideal gas and is close to 5/3. As example, for $Gr=6 \cdot 10^5$, the flow structure is completely dominated by one roll slightly distorted by the presence of two-linked left-vortices and two small right-vortices for low Knudsen number ($Kn=4.67 \cdot 10^{-5}$: macroscopic scale) where the macroscopic stream-function magnitude is close to 2.416. However, its value is close to 1.506 for a $Kn=2.80 \cdot 10^{-4}$ (going to the mesoscopic scale) and the flow pattern changes absolutely to asymmetric structure characterized by two counter-rotating large cells (see Fig. 10). Note here that for all computations the Mach number is less than 0.13.

7 Concluding remarks

We propose in this paper two LB models to be investigated and compared. The two models are rigorously selected from the most commonly used approaches in LBM based on some features, such as simplicity, accuracy, stability and computational cost. The predicted results show a high level of predictability for the two models compared to the referenced results. The model I based on two different lattices D2Q9-D2Q4 is found to be faster than the model II based on the simplified thermal energy model D2Q9-D2Q9, either for the standard forms and the accelerated forms. This difference is in fact due to the additionally algebraic operations taken by the model II in the collision process caused by the complex form of its energy distribution function.

We easily conclude on the high efficiency of the two preconditioned models; however, the use of the model I (passive scalar approach) in its standard or accelerated forms is extremely recommended. The preconditioned form of the model I has been, then, tested on two natural convection problems concerning symmetry breaking in low Prandtl number flows concerning crystal growth in enclosures. The corresponding results are compared to high order accurate solutions in available literature finding results and have shown good agreements with previous works for

transition thresholds. For high Grashof numbers ($Gr \geq 6 \cdot 10^5$), it has been found that the flow structure depends on the Knudsen number. We hope this work offers more explanations and help for researchers in the use the presented models as powerful and reliable tools in CFD.

Acknowledgement: This work has been done in very difficult conditions, in the days of the revolution of freedom of the Tunisian people against the dictatorial regime's authoritarian.

Appendix A

Chapman-Enskog analysis for the preconditioned internal energy equation:

The Taylor serie expansions result in:

$$h_\alpha = \sum_0^\infty \delta^n h_\alpha^{(n)} \tag{1}$$

$$\partial_t = \sum_0^\infty \delta^n \partial_{t_n} \tag{2}$$

By under zero'th, first and second orders we have:

$$O(\delta^0) : h_\alpha^{(0)} = h_\alpha^{eq} \tag{3}$$

$$O(\delta^1) : (\partial_{t_0} + e_{\alpha j} \partial_j) h_\alpha^{(0)} = -\frac{1}{\tau_h^*} h_\alpha^{(1)} \tag{4}$$

$$O(\delta^2) : \partial_{t_1} h_\alpha^{(0)} + (1 - \frac{1}{2\tau_h^*})(\partial_{t_0} + e_{\alpha j} \partial_j) h_\alpha^{(1)} = -\frac{1}{\tau_h^*} h_\alpha^{(2)} \tag{5}$$

Accounting for the summation (about α) constraints: $\sum_\alpha h_\alpha^{(0)} = \rho \epsilon$, $\sum_\alpha e_{\alpha j} h_\alpha^{(0)} = \Lambda_j^{(0)} = \rho V_j \epsilon / \gamma_h$, $\sum_\alpha h_\alpha^{(n \geq 1)} = 0$ and $\sum_\alpha e_{\alpha j} h_\alpha^{(n \geq 1)} = \Lambda_j^{(n)}$.

Zero'th order moment of equation 4-5 give:

$$\partial_{t_0}(\rho \epsilon) + \partial_j(\rho V_j \epsilon / \gamma_h) = 0 \tag{6}$$

$$\partial_{t_1}(\rho \epsilon) + (1 - \frac{1}{2\tau_h^*}) \nabla_j \cdot \Lambda_j^{(1)} = 0 \tag{7}$$

$$\text{Où } \Lambda_j^1 = \sum_\alpha e_{\alpha j} h_\alpha^{(1)}$$

First order moment of equation 5 give:

$$\partial_{t_0} \Lambda_j^{(0)} + \nabla_j \cdot \sum_{\alpha} e_{\alpha j} e_{\alpha j} h_{\alpha}^{(0)} = -\frac{1}{\tau_h^*} \Lambda_j^{(1)} \quad (8)$$

Replacing equation (8) in equation (7) gives:

$$\partial_{t_1} (\rho \varepsilon) = (\tau_h^* - \frac{1}{2}) \nabla_j \cdot \left(\partial_{t_0} \Lambda_j^{(0)} + \nabla_j \cdot \sum_{\alpha} e_{\alpha j} e_{\alpha j} h_{\alpha}^{(0)} \right) \quad (9)$$

Summing Eq. (8) + δ Eq. (11) with considering $\delta \equiv \delta t$, $c_s^2 (\tau_h^* - \frac{1}{2}) \delta t = \frac{\alpha}{\gamma_h}$,

$$\sum_{\alpha} e_{\alpha j} e_{\alpha j} h_{\alpha}^{(0)} = (c_s^*)^2 \rho \varepsilon, \partial_{t_0} \Lambda_j^{(0)} \approx O(Ma^3)$$

and neglecting all terms of order $O(Ma^3)$ or $O(Ma^2 \cdot \delta T)$, we finally obtain the preconditioned internal energy equation (applying the same procedure yields to the scalar equation):

$$\partial_t (\rho \varepsilon) + \partial_j (\rho V_j \varepsilon) / \gamma_h = \alpha \nabla_j^2 (\rho \varepsilon) / \gamma_h \quad (10)$$

The same procedure can be easily applied to the passive scalar approach.

References

- Azwadi, N.; Sidik, C.** (2007): The development of thermal lattice Boltzmann models in incompressible limit, *Journal of Fundamental Sciences*, n. 3, pp. 193-202.
- Ben Hadid, H.; Roux, B.** (1990): Buoyancy-driven oscillatory flows in shallow cavities filled with low-Prandtl number fluids, In Proc. GAMM Workshop on Numerical Solution of Oscillatory Convection in Low Prandtl Number Fluids (ed. B. Roux). *Notes on Numerical Fluid Mechanics*, vol. 27, pp. 25-33. Vieweg, Braunschweig.
- Bennacer, R.; El Ganaoui M.; Leonardi, E.** (2006): Symmetry breaking of melt flow typically encountered in a Bridgman configuration heated from below; *Applied Mathematical Modelling*, 30, pp. 1249-1261.
- Chatterjee, D.** (2010): Lattice Boltzmann simulation of incompressible transport phenomena in macroscopic solidification processes, *Num. Heat Transfer, Part B: Fundamentals*, vol. 58, Issue 1, pp. 55-72.
- Chew, Y. T.; Shu, C.; and X. D. Niu,** (2002): Simulation of unsteady incompressible flows by using Taylor Series expansion-and least square-based lattice Boltzmann method, *Int. J. of Modern Physics C*, vol. 13, n. 6, pp. 719-738.

de Vahl Davis, G. (1983): Natural convection of air in a square cavity: A benchmark numerical solutions, *Int. J. Numer. Methods Fluids*, n. 3, pp. 249-264.

Djebali, R.; El Ganaoui, M.; Sammouda, H.; Bennacer, R. (2009): Some benchmarks of a side wall heated cavity using lattice Boltzmann approach, *FDMP: Fluid Dynamics & Materials Processing*, vol.164, n. 1, pp. 1-21.

Djebali, R.; Pateyron, B.; El Ganaoui, M.; Sammouda, H. (2009): Axisymmetric high temperature jet behaviors based on a lattice Boltzmann computational method Part I: argon plasma, *Int. Rev. Chem. Eng.*, vol. 1, n. 5, pp. 428-438.

Djebali, R.; Sammouda, H.; El Ganaoui, M. (2010): Some advances in applications of lattice Boltzmann method for complex thermal flows; *Adv. Appl. Math. Mech.*, vol. 2, n. 5, pp. 587-608.

El Ganaoui, M.; Semma, E. A. (2009): A lattice Boltzmann coupled to finite volumes method for solving phase change problems, *Ther. Sci.* vol. 13, n. 2, pp. 205-216.

El Ganaoui, M.; Bontoux, P.; Lamazouade, A.; Leonardi, E.; de Vahl Davis, G. (2002): Computational model for solutal convection during directional solidification, *Num. Heat Transfer, Part B: Fundamentals*, vol. 41, Issue 3, pp. 325-338.

El Ganaoui, M.; Djebali, R. (2010): Aptitude of a lattice Boltzmann method for evaluating transitional thresholds for low Prandtl number flows in enclosures; *C. R. Mécanique* 338, pp. 85-96

Forth, S.C. and Staroselsky, A. (2005): A hybrid FEM/BEM approach for designing an aircraft engine structural health monitoring, *CMES: Computer Modeling in Engineering & Sciences*, vol.9, n.3, pp. 287-298.

Gelfgat, A. Y.; Bar-Yoseph, P. Z.; Yarin, A. L. (1999): Stability of multiple steady states of convection in laterally heated cavities, *J. Fluid Mech.*, vol. 388, pp. 315-334.

Guo, Z.; Zhao, T. S. (2005): A Lattice Boltzmann model for convection heat transfer in porous media, *Num. Heat Transfer, Part B: Fundamentals*, vol. 47, n. 2, pp. 157-177.

Guo, Z.; Zhao, T.S.; Shi, Y. (2004): Preconditioned lattice-Boltzmann method for steady flows, *Phys. Rev. E* 70, 066706.

Guo, Z.-L.; Shi, B.-C.; Zheng, C.-G. (2002) A coupled lattice BGK model for the Bouessinesq equation, *Int. J. Num. Meth. Fluids*, n. 39, pp. 325-342.

He, X.; Luo, L.S. (1997): Lattice Boltzmann model for the incompressible Navier-Stokes equation, *Journal of Statistical Physics*, vol. 88, n. 3/4, pp. 927-944.

Hui, G.; ChuiJie, W. (2009): Large-eddy simulations of turbulent flows with lat-

tice Boltzmann dynamics and dynamical system sub-grid models, *Sci. China Ser. E-Tech. Sci.* vol. 52, n. 3, pp. 670-679.

Larroudé, P.; Ouazzani, J. L.I.D. Alexander, P. Bontoux, (1994): Symmetry breaking low transitions and oscillatory flows in a 2D directional solidification model, *European Journal of Mechanics B*, 13 (3), pp. 353-381.

Le Quéré, P. (1991): Accurate solutions to the square thermally driven cavity at high Rayleigh number, *Computers Fluids*, vol. 20, n. 1, pp. 29-41.

Leung, C. H.; Berzins, M. (2003): A computational model for organism growth based on surface mesh generation, *J. of Comp. Physics*, vol. 188, Issue 1, pp. 75-99.

Liang, X.; Li, X.; Fu, D. and Ma, Y. (2009): Complex transition of double diffusive convection in a rectangular enclosure with height-to-length ratio equal to 4: Part I, *Commun. Comput. Phys.* vol. 6, n. 2, pp. 247-268.

Mohamad, A. A.; Kuzmin, A. (2010): A critical evaluation of force term in lattice Boltzmann method, natural convection problem, *Int. J. of Heat and Mass Transfer*, n.53, pp. 990-996.

Mohamad, A.A. (2007): Applied lattice Boltzmann method for transport phenomena, momentum, heat and mass transfer, Sure Print, Calgary.

Moon, J. K.; Kim, S. J. (2010): Parallel computing performance of thermal-structural coupled analysis in parallel computing resource, *CMES: Computer Modeling in Engineering & Sciences*, vol.67, n.3, pp. 239-264.

Naj, H.; Mompean, G. (2009): Computation of the turbulent flow in a square duct using a cubic low-Reynolds stress model, *CMES: Computer Modeling in Engineering & Sciences*, vol.53, n. 2 , pp. 181-206.

Peng, Y.; Shu, C.; Chew, Y. T. (2003): Simplified thermal lattice Boltzmann model for incompressible thermal flows, *Physical Review E* 68, 026701.

Premnath, K. N.; Pattison, M. J.; Banerjee, S. (2009): Steady state convergence acceleration of the generalized lattice Boltzmann equation with forcing term through preconditioning, *Journal of Computational Physics*, n. 228, pp. 746-769.

Pulicani, P. A.; del Arco, C.; Randriamampianina, A.; Bontoux, P.; Peyret, R. (1990): Spectral simulations of oscillatory convection at low Prandtl number, *Intl J. Numer. Methods Fluids*, 10, pp. 481-517.

Semma, A. (2004): Etude numérique des transferts de chaleur et de masse durant la croissance dirigée: effet de paramètres de contrôle, *Thèse de doctorat de l'Ecole Mohammadia d'Ingénieurs, Université Mohamed V, Maroc.*

Shu, C. X.; Niu, D.; Chew, Y. T. (2003): Taylor series expansion-and least square-based lattice Boltzmann method: three-dimensional formulation and its applica-

tions, *Int. J. of Modern Physics C*, vol. 14, n. 7, pp. 925-944.

Shu, C.; Ding, H.; Yeo, K.S. (2005): Computation of incompressible Navier-Stokes equations by local RBF-based differential quadrature method, *CMES: Computer Modeling in Engineering & Sciences*, vol.7, n.2, pp. 195-205

Shu, C.; Xue, H. (1998): Comparison of two approaches for implementing stream function boundary conditions in DQ simulation of natural convection in a square cavity, *Int. J. Heat & Fluid Flow*, n. 19, pp. 59-68.

Tsukiji, T.; Yamamoto, Y. (2005): Computational modeling of gas-particle two-phase jet by a 3-D vortex method, *CMES: Computer Modeling in Engineering & Sciences*, vol.9, n. 3, pp. 235-242.

Winters, K.H. (1988): Oscillatory convection in liquid metals in a horizontal temperature gradient, *Int J. Numer. Methods Engng*, 25, pp. 401-414.

Winters, K.H. (1990): A bifurcation analysis of oscillatory convection in liquid metals. Proc. GAMM Workshop on Numerical Solution of Oscillatory Convection in Low Prandtl Number Fluids (ed. B. Roux). *Notes on Numerical Fluid Mechanics*, vol. 27, pp. 319-326, Vieweg, Braunschweig.